$\tau > 5$ ms, a second peak emerges within our detectable range near $1/\mu m < k < 1.5/\mu m$. The signal-to-noise ratios for the peaks are statistically limited to 1 to 2 for images taken at a fixed hold time. Combining data points at all times, one recovers clear oscillations as observed in Fig. 2B. The multiple peaks and troughs in momentum space result from the interference of sound waves with different wavelengths and are the key features of Sakharov oscillations in the angular spectrum of the CMB radiation. Moreover, moving acoustic peaks as time evolves suggests that the correlations are spreading out at a finite speed of sound. For the quench-up experiments, the oscillations are less clear, owing to the limited imaging resolution and the sample size. Nonetheless, we clearly observe that correlations are suppressed at smaller k as time evolves. Spreading of correlations along the acoustic "light-cone" was also reported in a quenched atomic Mott insulator (*26*).

The oscillations in the time and space domains can be understood as the interference of counter-propagating phonon pairs $\hat{b}^{\dagger}_{\pm k} e^{\pm ikr - i\epsilon(k)\tau/h}$, where $\hat{b}^{\dagger}_{\pm k}$ is the creation operator of phonons with momentum $\pm k$ and energy $\epsilon(k)$. Assuming that phonons are long-lived, the structure factor follows a simple form (*10*, *20*), $S(k,\tau) = S(k,0) + 2B_k \cos\phi \sin^2(\pi f\tau)$, where $B_k > 0$ is the oscillation amplitude, the oscillation frequency is given by $f(k) = 2\epsilon(k)/h$, and the relative phase is $\phi = 0$ for quench-up experiments and $\phi = \pi$ for quench-downs (*20*). Adopting sinusoidal fits to the measured data in Fig. 2, we determine the oscillation frequencies for various k and g_f. The result in turn provides good fits to the data shown in Fig. 3 (*20*).

We summarize five sets of measurements on quenched superfluids and compare the oscillation frequencies to the predictions from the Bogoliubov theory: $\epsilon(k) = v\hbar k\sqrt{1+k^2\xi^2/4}$, where $v = \hbar\sqrt{\tilde{n}g_f}/m$ is the speed of sound and $\xi = \hbar/mv$ is the healing length. Plotting the frequencies in the dimensionless units based on calculated v and ξ, the data in all three quench-down measurements collapse to a single curve, which agrees with the Bogoliubov theory (Fig. 4B). Quench-up experiments, however, show consistently 65% higher frequencies than the prediction (Fig. 4A). The discrepancy likely results from the effects of strong initial density fluctuations in quench-up experiments and finite temperature (*20*).

The space-time dependence of the density correlations in quenched superfluids not only supports the picture of Sakharov acoustic oscillations, but also suggests that Sakharov oscillation is a universal feature of a quenched hydrodynamic system far from thermal equilibrium. The time and spatial scales of the oscillations are related by the speed of sound v, and the observed propagation of Sakharov acoustic peaks is consistent with the sonic horizon $k = \pi/v\tau$ within which the waves can interfere. In particular, good agreement with the Bogoliubov theory is found when the interaction is quenched to smaller values, and the growing multipeak structure in the density noise power spectrum resembles that in the CMB radiation spectrum. The observation of Sakharov oscillations in a quenched atomic superfluid raises prospects of investigating universal hydrodynamic phenomena in a laboratory setting, as well as of extending the current experimental tools to address exciting topics in cosmology and gravitational physics such as Hawking radiation (*13*) or Unruh effect (*27*).

References and Notes

1. A. D. Sakharov, *Sov. Phys. JETP* **49**, 345 (1965).
2. Ya. B. Zeldovich, I. D. Novikov, *Relativistic Astrophysics* (Univ. of Chicago Press, Chicago, 1983), vol. 2.
3. D. Larson *et al.*, *Astrophys. J. Suppl. Ser.* **192**, 16 (2011).
4. D. J. Eisenstein *et al.*, *Astrophys. J.* **633**, 560–574 (2005).
5. P. J. E. Peebles, J. T. Yu, *Astrophys. J.* **162**, 815 (1970).
6. R. A. Sunyaev, Ya. B. Zel'dovich, *Astrophys. Space Sci.* **7**, 3 (1970).
7. J. R. Bond, G. Efstathiou, *Astrophys. J.* **285**, L45 (1984).
8. W. Hu, S. Dodelson, *Annu. Rev. Astron. Astrophys.* **40**, 171–216 (2002).
9. D. J. Eisenstein, C. L. Bennett, *Phys. Today* **61**, 44 (2008).
10. L. P. Grishchuk, *Usp. Fiziol. Nauk* **182**, 222 (2012).
11. C. J. Pethick, H. Smith, *Bose-Einstein Condensation in Dilute Gases* (Cambridge Univ. Press, Cambridge, 2008).
12. W. G. Unruh, *Phys. Rev. Lett.* **46**, 1351–1353 (1981).
13. L. J. Garay, J. R. Anglin, J. I. Cirac, P. Zoller, *Phys. Rev. Lett.* **85**, 4643–4647 (2000).
14. P. O. Fedichev, U. R. Fischer, *Phys. Rev. A* **69**, 033602 (2004).
15. M. Uhlmann, Y. Xu, R. Schützhold, *New J. Phys.* **7**, 248 (2005).
16. A. Imambekov *et al.*, *Phys. Rev. A* **80**, 033604 (2009).
17. J.-C. Jaskula *et al.*, *Phys. Rev. Lett.* **109**, 220401 (2012).
18. O. Lahav *et al.*, *Phys. Rev. Lett.* **105**, 240401 (2010).
19. C. Chin, R. Grimm, P. Julienne, E. Tiesinga, *Rev. Mod. Phys.* **82**, 1225–1286 (2010).
20. Materials and methods are available as supplementary materials on *Science* Online.
21. S. S. Natu, E. J. Mueller, *Phys. Rev. A* **87**, 053607 (2013).
22. C.-L. Hung, X. Zhang, N. Gemelke, C. Chin, *Nature* **470**, 236–239 (2011).
23. D. S. Petrov, M. Holzmann, G. V. Shlyapnikov, *Phys. Rev. Lett.* **84**, 2551–2555 (2000).
24. C.-L. Hung *et al.*, *New J. Phys.* **13**, 075019 (2011).
25. T. Yefsah, R. Desbuquois, L. Chomaz, K. J. Günter, J. Dalibard, *Phys. Rev. Lett.* **107**, 130401 (2011).
26. M. Cheneau *et al.*, *Nature* **481**, 484–487 (2012).
27. A. Retzker, J. I. Cirac, M. B. Plenio, B. Reznik, *Phys. Rev. Lett.* **101**, 110402 (2008).

Acknowledgments: We are grateful to L. Radzihovsky, W. Hu, and C.-L. Kuo for helpful discussions. We thank X. Zhang, L.-C. Ha, and S.-K. Tung for the laboratory support. C.-L.H. and C.C. are supported by NSF award PHY-1206095, Army Research Office grant W911NF0710576 with funds from the Defense Advanced Research Projects Agency OLE Program, and the Packard foundation. V.G. is supported by NSF awards PHY-1211914 and DMR-1205303. The data presented in this paper are available upon request sent to cchin@uchicago.edu.

Supplementary Materials

www.sciencemag.org/cgi/content/full/science.1237557/DC1
Materials and Methods
References (*28*–*30*)

8 March 2013; accepted 24 July 2013
Published online 1 August 2013;
10.1126/science.1237557

An Atomic Clock with 10^{-18} Instability

N. Hinkley,[1,2] J. A. Sherman,[1] N. B. Phillips,[1] M. Schioppo,[1] N. D. Lemke,[1] K. Beloy,[1] M. Pizzocaro,[1,3,4] C. W. Oates,[1] A. D. Ludlow[1]*

Atomic clocks have been instrumental in science and technology, leading to innovations such as global positioning, advanced communications, and tests of fundamental constant variation. Timekeeping precision at 1 part in 10^{18} enables new timing applications in relativistic geodesy, enhanced Earth- and space-based navigation and telescopy, and new tests of physics beyond the standard model. Here, we describe the development and operation of two optical lattice clocks, both using spin-polarized, ultracold atomic ytterbium. A measurement comparing these systems demonstrates an unprecedented atomic clock instability of 1.6×10^{-18} after only 7 hours of averaging.

Quantum mechanical absorbers such as atoms serve as the best available time and frequency references: They are isolatable, possess well-defined transition frequencies, and exist in abundant identical copies. With more than 50 years of development, clocks based on microwave oscillators referenced to atomic transitions now define the Système International (SI) second and play central roles in network synchronization, global positioning systems, and tests of fundamental physics (*1*, *2*). Under development worldwide, optical clocks oscillate 10^5 times faster than their microwave predecessors, dividing time into finer intervals (*3*). Although microwave clocks such as the Cs fountain have demonstrated time and frequency measurements of a few parts in 10^{16} (*4*, *5*), optical clocks now measure with a precision of 1 part in 10^{17} (*6*–*9*).

A clock's instability specifies how its ticking fluctuates over time, a characteristic generally quantified by the Allan deviation (*10*). No time or frequency standard can make measurements

[1]National Institute of Standards and Technology (NIST), 325 Broadway, Boulder, CO 80305, USA. [2]Department of Physics, University of Colorado, Boulder, CO 80309, USA. [3]Instituto Nazionale di Ricerca Metrologica, Strada delle Cacce 91, 10135 Torino, Italy. [4]Politecnico di Torino, Corso duca degli Abruzzi 24, 10125 Torino, Italy.

*Corresponding author. E-mail: ludlow@boulder.nist.gov

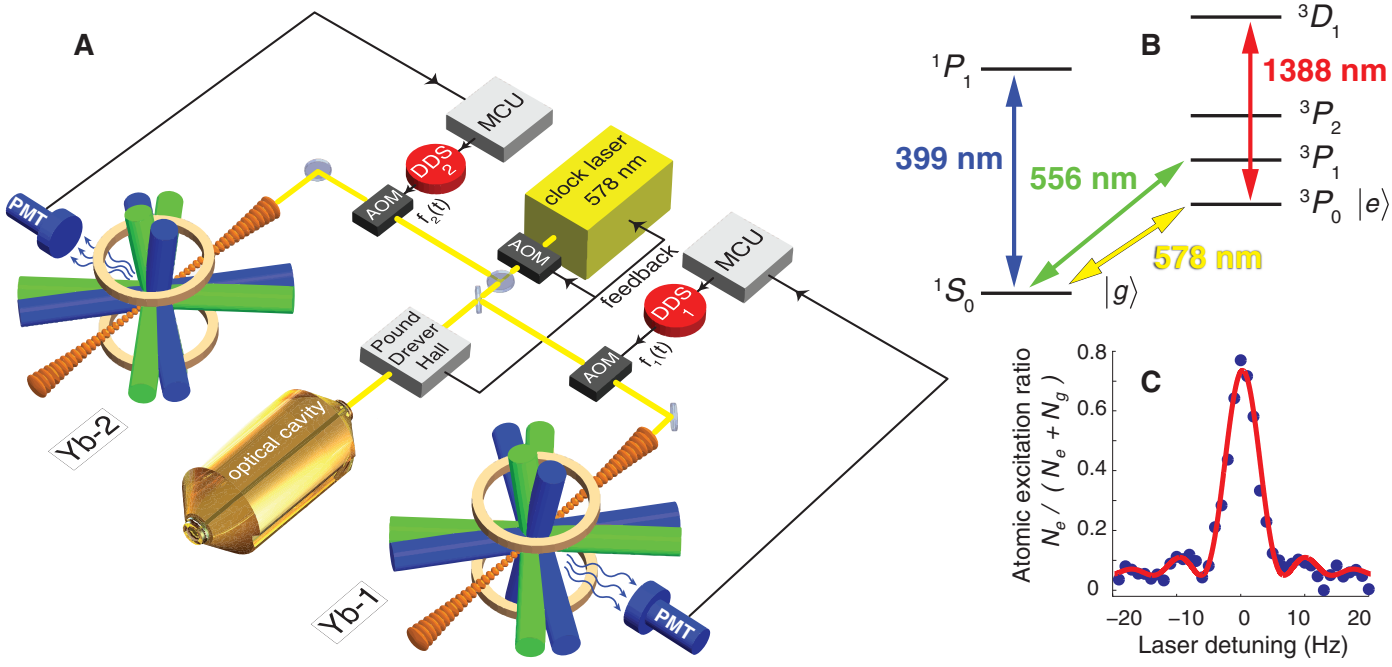

Fig. 1. Experimental realization of the Yb optical lattice clocks. (A) Laser light at 578 nm is prestabilized to an isolated, high-finesse optical cavity using Pound-Drever-Hall detection and electronic feedback to an AOM and laser piezoelectric transducer. Fibers deliver stabilized laser light to the Yb-1 and Yb-2 systems. Resonance with the atomic transition is detected by observing atomic fluorescence collected onto a PMT. The fluorescence signal is digitized and processed by a microcontroller unit (MCU), which computes a correction frequency, $f_{1,2}(t)$. This correction frequency is applied to the relevant AOM by way of a direct digital synthesizer (DDS) and locks the laser frequency onto resonance with the clock transition. **(B)** Relevant Yb atomic energy levels and transitions, including laser-cooling transitions (399 and 556 nm), the clock transition (578 nm), and the optical-pumping transition used for excited-state detection (1388 nm). **(C)** A single-scan, normalized excitation spectrum of the $^1S_0$-$^3P_0$ clock transition in ^{171}Yb with 140-ms Rabi spectroscopy time; the red line is a free-parameter sinc^2 function fit.

Fig. 2. Frequency comparison between the Yb optical lattice clocks. (A) Correction frequencies, $f_{1,2}(t)$, are shown in red and black. Dominant LO fluctuations are due to the cavity and are, thus, common to the atomic systems. **(B)** Frequency difference, $f_2(t) - f_1(t)$, between the two Yb clock systems for a 5000-s interval. **(C)** Data set $f_2(t) - f_1(t)$ over a 90,000-s interval. Gaps represent data rejected before data analysis due to servo unlocks. **(D)** Histogram of all data and a Gaussian fit ($\chi^2_r = 0.9996$).

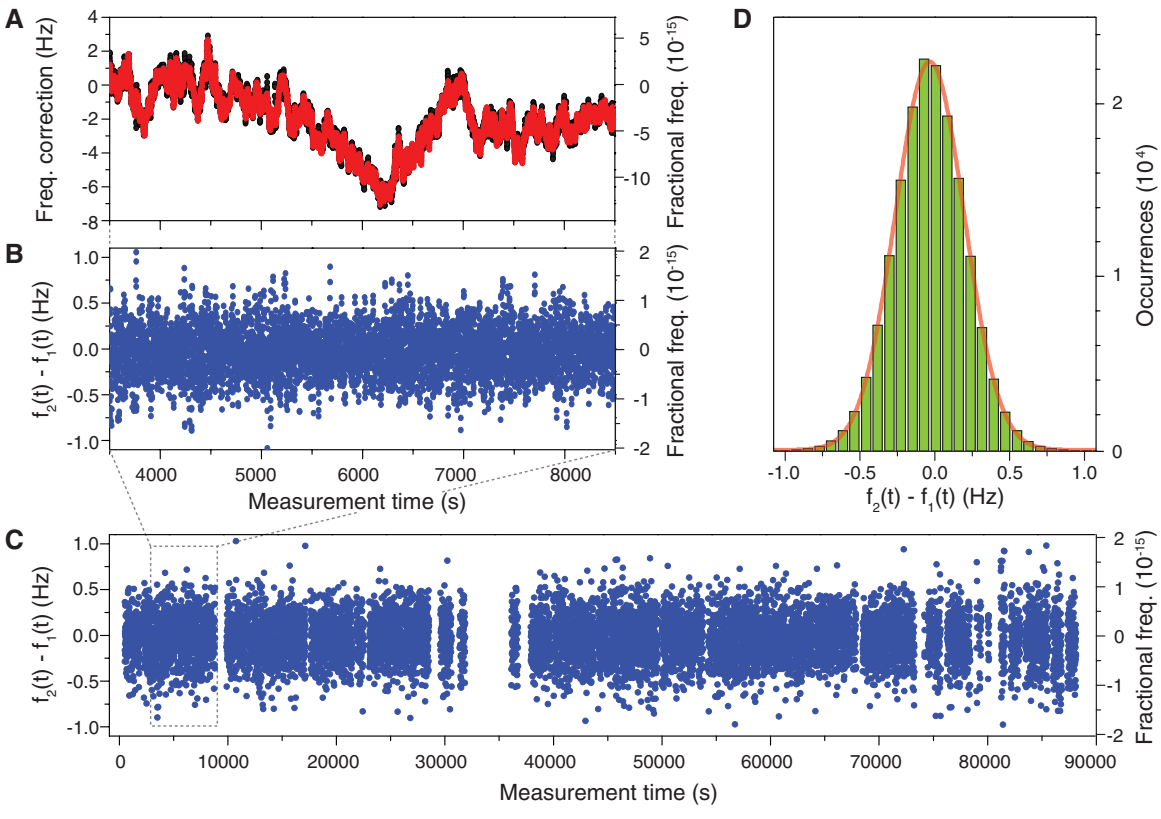

better than the statistical precision set by its instability. Further, a clock's systematic uncertainty is often constrained by its long-term instability. For these reasons, and because many timing applications require only exquisite instability, the instability represents perhaps the most important property of an atomic standard.

In pursuit of lower instability, an optical lattice clock uses a stabilized laser referenced to many (10^3 to 10^6) alkaline earth (or similar) atoms confined in an optical standing wave. Alignment of the clock interrogation laser along the direction of tight lattice confinement eliminates most Doppler and motional effects while probing the ultranarrow-band electronic clock transition. These atoms are interrogated simultaneously, improving the atomic detection signal-to-noise ratio and, thus, instability, which is limited fundamentally by quantum projection noise (QPN) (*11*). Like other cycled atomic clocks, the lattice clock suffers from a technical noise source known as the Dick effect, arising when an oscillator's noise is periodically sampled (*12*, *13*). Cavity-stabilized lasers with low thermal noise have reduced the Dick effect, enabling clock instability below 10^{-15} at short times (*14*). Recently, an uncorrelated comparison of two strontium lattice clocks revealed clock instability of 3×10^{-16} at short times, averaging to 1×10^{-17} in 1000 s (*8*) or, in another case, reaching the 10^{-17} level in 20,000 s (*9*). Here, by comparing two independent optical lattice clocks using ultracold ^{171}Yb, we demonstrate a clock instability of 1.6×10^{-18} in 25,000 s.

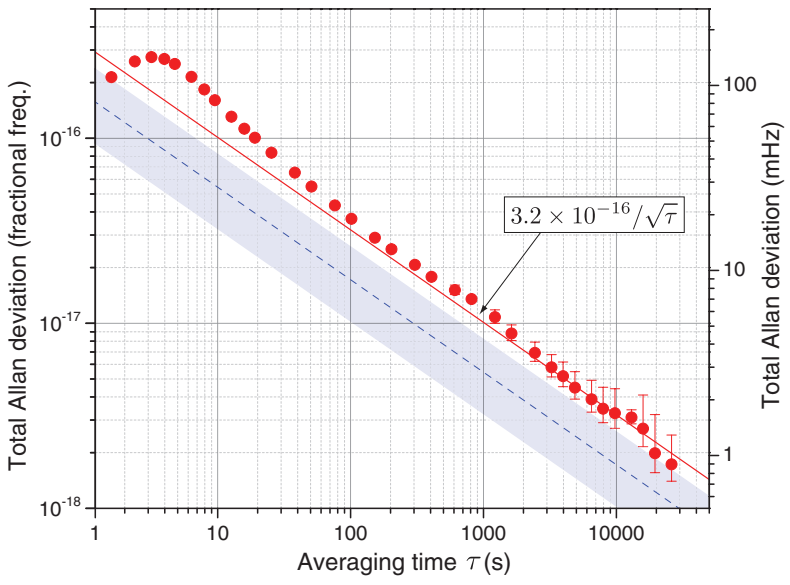

Fig. 3. Measured instability of a Yb optical lattice clock. Total Allan deviation of a single Yb clock, $[f_2(t) - f_1(t)]/\sqrt{2}$ (red circles), and its white-frequency-noise asymptote of $3.2 \times 10^{-16}/\sqrt{\tau}$ (red solid line). The blue dashed line represents the estimated combined instability contributions from the Dick effect ($1.4 \times 10^{-16}/\sqrt{\tau}$) and QPN ($1 \times 10^{-16}/\sqrt{\tau}$); the shaded region denotes uncertainty in these estimates. Error bars indicate 1σ confidence intervals.

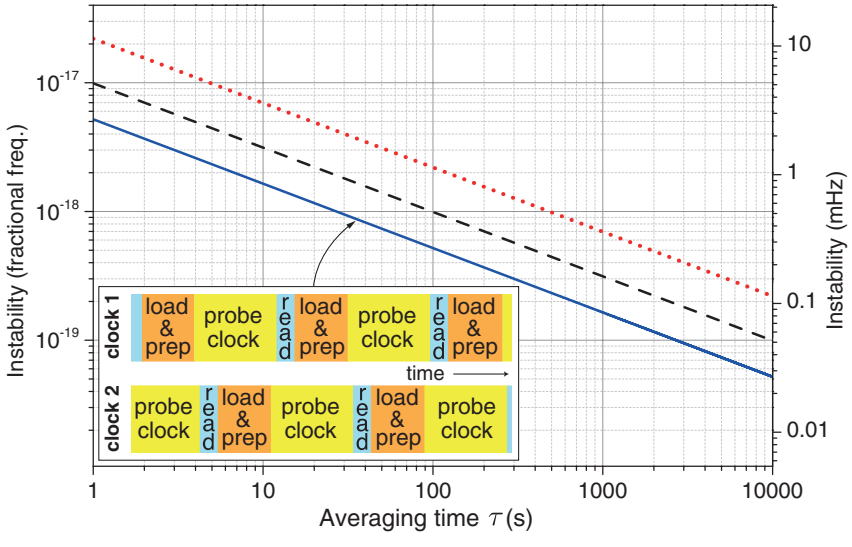

Fig. 4. Calculated instability limits toward the goal of 1×10^{-18} in 100 s. The Dick limit (red dotted line) is reduced by using a hypothetical LO four times as stable as the LO used in our experiment. The QPN limit is shown under the same conditions (black dashed line), assuming 50,000 atoms. The inset illustrates an interleaved interrogation of two atomic systems, allowing continuous monitoring of the LO for suppression of the Dick effect. Dead times from atomic preparation or readout in one system are synchronized with clock interrogation in the second system. The solid blue line indicates the suppressed Dick instability in the interleaved interrogation scheme using Ramsey spectroscopy with an unimproved LO.

Both clock systems, referred to here as Yb-1 and Yb-2, independently cool and collect ^{171}Yb atoms from thermal beams into magneto-optical traps [see Fig. 1 and (*15*)]. Two stages of laser cooling, first on the strong $^1S_0$-$^1P_1$ cycling transition at 399 nm, followed by the weaker $^1S_0$-$^3P_1$ intercombination transition at 556 nm, reduce the atomic temperature from 800 K to 10 μK. Each cold atom sample is then loaded into an optical lattice with ~300E_r trap depth (E_r/k_B = 100 nK; E_r, recoil energy; k_B, Boltzmann's constant) formed by retroreflecting ~600 mW of laser power, fixed at the "magic" wavelength $\lambda_m \approx 759$ nm (*16*) by a reference cavity. At λ_m, both electronic states of the clock transition are Stark-shifted equally (*17*, *18*). For the measurements described here, ~5000 atoms captured by each lattice are then optically pumped to one of the two ground-state spin projections $m_F = \pm 1/2$ using the $^1S_0$-$^3P_1$ transition. After this state preparation, applying a 140-ms-long π pulse of 578-nm light resonant with the $^1S_0$-$^3P_0$ clock transition yields the spectroscopic line shape shown in Fig. 1C, with a Fourier-limited linewidth of 6 Hz. Experimental clock cycles alternately interrogate both m_F spin states canceling first-order Zeeman and vector Stark shifts. The optical local oscillator (LO) is an ultrastable laser servo-locked to a high-finesse optical cavity (*14*) and is shared by both Yb systems. Light is frequency-shifted into resonance with the clock transition of each atomic system by independent acousto-optic modulators (AOMs). Resonance is detected by monitoring the $^1S_0$ ground-state population (N_g) and $^3P_0$ excited-state population (N_e). A laser cycles ground-state atoms on the $^1S_0$-$^1P_1$ transition while a photomultiplier tube (PMT) collects the fluorescence, giving a measure of N_g. After 5 to 10 ms of cycling, these atoms are laser-heated out of the lattice. At this point, N_e is optically pumped to the lowest-lying $^3D_1$ state, which decays back to the ground state. The $^1S_0$-$^1P_1$ transition is cycled again, now measuring N_e. Combining these measurements yields a normalized mean excitation $N_e/(N_e + N_g)$. During spectroscopy, special attention was paid to

eliminating residual Stark shifts stemming from amplified spontaneous emission of the lattice lasers, eliminating residual Doppler effects from mechanical vibrations of the apparatus correlated with the experimental cycle, and controlling the cold collision shift due to atomic interactions within the lattice (*19*).

By measuring the normalized excitation while modulating the clock laser frequency by ±3 Hz, an error signal is computed for each Yb system. Subsequently, independent microprocessors provide a digital frequency correction $f_{1,2}(t)$ at time t to their respective AOMs, thereby maintaining resonance on the line center. In this way, though derived from the same LO, the individual laser frequencies for Yb-1 and Yb-2 are decoupled and are instead determined by their respective atomic samples (for all but the shortest time scales). The frequency correction signals $f_{1,2}(t)$ are shown in Fig. 2A for a 5000-s interval. Because the experimental cycles for each clock system are unsynchronized and have different durations, $f_{1,2}(t)$ signals are interpolated to a common time base and subtracted to compute the frequency difference between Yb-1 and Yb-2, as shown in Fig. 2, B to D. Measurements such as these were repeated several times for intervals of ~15,000 s, demonstrating a clock instability reaching 4×10^{-18} at 7500 s. While collecting data over a 90,000-s interval, we observed the instability curve in Fig. 3, shown as the total Allan deviation for a single Yb clock. Before data analysis, ~25% of the attempted measurement time was excluded due to laser unlocks and auxiliary servo failures (*15*). Each clock servo had an attack time of a few seconds, evidenced by the instability bump near 3 s. At averaging times $\tau = 1$ to 5 s, the instability is comparable to previous measurements (*14*) of the free-running laser system, and at long times, the instability averages down like white frequency noise as $\sim 3.2 \times 10^{-16}/\sqrt{\tau}$ (for τ in seconds), reaching 1.6×10^{-18} at 25,000 s.

Also shown in Fig. 3 is an estimate of the combined instability contribution (blue dashed line) from the Dick effect and QPN (shaded region denotes the uncertainty of the estimate). These contributions must be reduced if 10^{-18} instability is desired at time scales under 100 s. Substantial reductions of QPN are possible with the use of higher atom numbers and longer interrogation times. Further stabilization of the optical LO will continue to reduce the Dick effect, by both lowering the laser frequency noise down-converted in the Dick process and allowing increased spectroscopy times for higher duty cycles. Improved LOs will use optical cavities exhibiting reduced Brownian thermal-mechanical noise by exploiting cryogenic operation (*20*), crystalline optical coatings (*21*), longer cavities, or other techniques (*14*). Figure 4 demonstrates the advantage of improving the present LO, with four times less laser frequency noise and four times longer interrogation time (corresponding to a short-term laser instability of $\sim 5 \times 10^{-17}$). The red dotted line gives the Dick instability, whereas the black dashed line indicates the QPN limit, assuming a moderate 50,000 atom number.

Noting that the calculated Dick effect remains several times higher than the QPN limit, we consider an alternative idea first proposed for microwave ion clocks: interleaved interrogation of two atomic systems (*13*). By monitoring the LO laser frequency at all times with interleaved atomic systems, the aliasing problem at the heart of the Dick effect can be highly suppressed. The solid blue line in Fig. 4 illustrates the potential of a simple interleaved clock interrogation using Ramsey spectroscopy. Even with the present LO, the Dick effect is decreased well below the QPN limit afforded by a much-improved LO (black dashed line). In this case, spin squeezing of the atomic sample could reduce the final instability beyond the standard quantum limit set by QPN (*22*). The two-system, interleaved technique requires spectroscopy times that last one half or more of the total experimental cycle. By extending the Yb clock Ramsey spectroscopy time to >250 ms, we achieved a 50% duty cycle for each system, demonstrating the feasibility of this technique. Further suppression of the Dick effect can be achieved with the use of a more selective interleaving scheme. Duty cycles ≥50% can also be realized with the aid of nondestructive state detection (*23*).

Another important property of a clock is its accuracy, which results from uncertainty in systematic effects that alter a standard's periodicity from its natural, unperturbed state. In 2009, we completed a systematic analysis of Yb-1 at the 3×10^{-16} uncertainty level (*16*). Since then, we reduced the dominant uncertainty due to the blackbody Stark effect by one order of magnitude (*24*). With its recent construction, Yb-2 has not yet been systematically evaluated. The fact that the instability reaches the 10^{-18} level indicates that key systematic effects (e.g., the blackbody Stark effect, atomic collisions, lattice light shifts) on each system are well controlled over the relevant time scales. The mean frequency difference in Fig. 2 was $\langle f_2(t) - f_1(t) \rangle = -30$ mHz, which is within the Yb-1 uncertainty at 10^{-16}. Systematic effects on each system can now be efficiently characterized beyond the 10^{-17} level. With continued progress, we envision 10^{-18} instability in only 100 s and long-term instability well below 10^{-18}.

Clock measurement at the 10^{-18} level can be used to resolve spatial and temporal fluctuations equivalent to 1 cm of elevation in Earth's gravitational field (*25*–*28*), offering a new tool for geodesy, hydrology, geology, and climate change studies. Space-based implementations can probe alternative gravitational theories, e.g., by measuring red-shift deviations from general relativity with a precision that is three orders of magnitude higher than the present level (*28*). Though present-day temporal and spatial variation of fundamental constants is known to be small (*6*, *29*, *30*), 10^{-18}-level clock measurements can offer tighter constraints. Finally, timekeeping improvements can benefit navigation systems, telescope array synchronization (e.g., very-long-baseline interferometry), secure communication, and interferometry and can possibly lead to a redefinition of the SI second (*9*).

References and Notes

1. A. Bauch, *Meas. Sci. Technol.* **14**, 1159–1173 (2003).
2. J. Levine, *Rev. Sci. Instrum.* **70**, 2567–2596 (1999).
3. S. A. Diddams, J. C. Bergquist, S. R. Jefferts, C. W. Oates, *Science* **306**, 1318–1324 (2004).
4. J. Guena *et al.*, *IEEE Trans. Ultra. Ferro. Freq. Cont.* **59**, 391–409 (2012).
5. T. E. Parker, *Metrologia* **47**, 1–10 (2010).
6. T. Rosenband *et al.*, *Science* **319**, 1808–1812 (2008).
7. C. W. Chou, D. B. Hume, J. C. J. Koelemeij, D. J. Wineland, T. Rosenband, *Phys. Rev. Lett.* **104**, 070802 (2010).
8. T. L. Nicholson *et al.*, *Phys. Rev. Lett.* **109**, 230801 (2012).
9. R. Le Targat *et al.*, *Nat. Commun.* **4**, 2109 (2013).
10. C. A. Greenhall, D. A. Howe, D. B. Percival, *IEEE Trans. Ultra. Ferro. Freq. Cont.* **46**, 1183–1191 (1999).
11. W. M. Itano *et al.*, *Phys. Rev. A* **47**, 3554–3570 (1993).
12. G. Santarelli *et al.*, *IEEE Trans. Ultra. Ferro. Freq. Cont.* **45**, 887–894 (1998).
13. G. J. Dick, J. D. Prestage, C. A. Greenhall, L. Maleki, in *Proceedings of the 22nd Precise Time and Time Interval Meeting* (NASA Conference Publication 3116, Washington, DC, 1990), pp. 487–508.
14. Y. Y. Jiang *et al.*, *Nat. Photon.* **5**, 158–161 (2011).
15. See supplementary materials on *Science* Online.
16. N. D. Lemke *et al.*, *Phys. Rev. Lett.* **103**, 063001 (2009).
17. J. Ye, H. J. Kimble, H. Katori, *Science* **320**, 1734–1738 (2008).
18. H. Katori, M. Takamoto, V. G. Pal'chikov, V. D. Ovsiannikov, *Phys. Rev. Lett.* **91**, 173005 (2003).
19. N. D. Lemke *et al.*, *Phys. Rev. Lett.* **107**, 103902 (2011).
20. T. Kessler *et al.*, *Nat. Photon.* **6**, 687–692 (2012).
21. G. D. Cole, W. Zhang, M. J. Martin, J. Ye, M. Aspelmeyer, *Nat. Photon.* **7**, 644–650 (2013).
22. I. D. Leroux, M. H. Schleier-Smith, V. Vuletić, *Phys. Rev. Lett.* **104**, 073602 (2010).
23. P. G. Westergaard, J. Lodewyck, P. Lemonde, *IEEE Trans. Ultra. Ferro. Freq. Cont.* **57**, 623–628 (2010).
24. J. A. Sherman *et al.*, *Phys. Rev. Lett.* **108**, 153002 (2012).
25. S. Schiller *et al.*, *Nucl. Phys. B Proc. Suppl.* **166**, 300–302 (2007).
26. C. W. Chou, D. B. Hume, T. Rosenband, D. J. Wineland, *Science* **329**, 1630–1633 (2010).
27. D. Kleppner, *Phys. Today* **59**, 10 (2006).
28. S. Schiller *et al.*, *Exp. Astron.* **23**, 573–610 (2009).
29. T. Chiba, *Prog. Theor. Phys.* **126**, 993–1019 (2011).
30. S. Blatt *et al.*, *Phys. Rev. Lett.* **100**, 140801 (2008).

Acknowledgments: We thank the Defense Advanced Research Projects Agency Quantum Assisted Sensing and Readout program, NASA Fundamental Physics, and NIST for financial support; D. Hume for experimental assistance; and T. Fortier and S. Diddams for femtosecond optical frequency comb measurements.

Supplementary Materials

www.sciencemag.org/cgi/content/full/science.1240420/DC1
Supplementary Text
Table S1

13 May 2013; accepted 12 August 2013
Published online 22 August 2013;
10.1126/science.1240420